# An Unknown Input Observer-EFIR Combined Estimator for Electro-Hydraulic Actuator in Sensor Fault Tolerant Control Application

Syed Abu Nahian, Dinh Quang Truong, Hoang Vu Dao, and Kyoung Kwan Ahn

***Abstract*—This paper presents a novel unknown input observer (UIO) integrated extended finite impulse response (EFIR) estimator (UIOEFIR) and its application for an effective sensor fault tolerant control of an electro-hydraulic-actuator (EHA). The proposed estimator exploits the UIO structure in the EFIR filter. Thus, it requires only a small number of historical data ($N$) whilst ensuring threefold: i) Sensor fault and system-state estimation accuracy under time-correlated noise ii) The number of estimator-design-parameters is significantly minimized. iii) Robust residual generation. A Lyapunov-stability-based theory is carried out to study its convergence condition. Next, an EHA-based test rig has been setup and sensor FTC is performed by carrying this estimator as a part of fault diagnosis algorithm to evaluate its performance by both simulation and real-time experiments. Results highlight that under optimal setting ($N = N_{opt}$), the estimator performance is near-accurate to the very-well-developed Extended Kalman Filter-based unknown input observer in an undisturbed conditions but significantly outperformed while dealing with time-correlated noise under the same control environment. The estimator also shows its robustness under below-optimal setting (downgrading $N_{opt}$ by *50%*.) while performing in real-time sensor fault-tolerant control.**

***Index Terms*—Extended finite impulse response (EFIR), fault-tolerant control, electro-hydraulic actuators, fault detection algorithm (FDA), unknown input observer.**

## I. Introduction

ELECTRO-HYDRAULIC actuators (EHAs) are well-known in modern industries for their compact size and ability to perform precise trajectory/high-pressure-based control tasks [1] in harsh environments. Meanwhile, depending on applications, sensor faults can be raised at any time while performing in closed-loop control logic for many reasons. Such incidents lead to control-instability and can result in major catastrophes. One smart way to avoid such failure is by observing the controlled variable using other state-measurements [2, 3]. However, the control performance may be seriously affected if the fault raises in the relying sensors. Therefore, researchers have focused on developing techniques for estimating the true states under multi-sensor fault condition and perform sensor FTC [4-8].

Syed Abu Nahian is a Project Engineer of WMG, University of Warwick, Coventry, CV4 7AL, United Kingdom. e-mail: S.Nahian@warwick.ac.uk

Dinh Quang Truong is an Assistant Professor of the University of Warwick, Coventry, CV4 7AL, United Kingdom. e-mail: T.Dinh@warwick.ac.uk

Hoang Vu Dao is the PhD candidate, Ulsan University, S. Korea

Kyoung Kwan Ahn is the Professor of Mechanical Engineering Department, Ulsan University, Ulsan, 680749 South Korea e-mail: kkahn@ulsan.ac.kr

A basic step of designing an FTC for any system is to develop an effective fault diagnosis algorithm (FDA) with three primary objectives: fault detection, fault isolation (location of fault), and fault identification (characteristic of the fault) [6]. Finally, based on appropriate FDA outcomes, control law(s) should be granted to manage the faulty condition. In general, two approaches of the FDA can be distinguished: i) Model-based approaches [3, 4], and ii) Data-driven approaches [7,8]. Presently, model-based FDA using observers and estimators have great significance as system states can be estimated by engaging the system-dynamics effectively [9-11]. In contrast, data-driven approaches utilize high dimensional results to make any decision [12]. For example, an innovative model-free neural network (NN)-based active fault-tolerant control scheme was proposed in [8]. Despite its nonlinear tracking superiority, the technique is difficult to implement for multi-state fault diagnosis because the designers need to define the parameter adaptation and control laws for each state in nominal condition. Additionally, the learning performance and the architecture of the NN could be hard to be decided if the system contains switched-nonlinearities like EHA [13].

In the recent past, researchers proposed several model-based sensor FDAs using state-observers. Back in the early 1970s, Unknown Input Observer (UIO) was proposed for robust fault diagnosis which could estimate time-varying unknown input value [14, 15]. Additionally, fault diagnosis using robust residual generation was performed by many researchers. Such as LMI optimization method was carried out by Wu and Jiang [9] and extended their research in the squirrel-cage induction motor application [10]. Robust observers like $H\infty$ , sliding mode observer/estimator-based fault diagnosis mechanisms were also studied in [4, 16]. Multi-fault detection and diagnosis using robust observers was also carried out in [17]. Intelligent or agent-based FDA for different nonlinear systems established in [11, 18-20]. In the EHA applications, Fu studied fault diagnosis of a large forging hydraulic press by extracting and mapping leakage information [21]. Intelligent and optimization-based fault diagnosis of EHA can also be found in several literatures [22, 23]. Though many of the above-mentioned studies proposed powerful strategies for different fault scenarios, noise disturbances were forcedly kept at its upper or lower boundary and required much design effort (such as the requirement of high-dimensional optimization tools in the design process). In some studies, process or measurement noise(s) were not taken under consideration inside the observer dynamics which can bias the estimation performance. Surely,

in the unconstrained environment definition, it is a challenge to estimate individual system state and fault characteristics with defective sensor outputs. To tackle noise-related problems, a nonlinear version of the Kalman filter (KF), the so-called extended Kalman filter (EKF), has been a popular tool for process fault diagnosis applications, including the EHA [24, 25]. Recently, the UIO adapted modified KF/EKFs was proposed in various fault detection, diagnosis and state estimation applications [26, 27]. By these methods, system states and unknown fault estimations under defective sensors can be efficiently performed. Despite their effectiveness, utilization of these estimators as a part of the EHA-FDAs still have important drawbacks due to its infinite-impulse-response (IIR) structure:

- They suffer from biased estimation as process noises can be non-additive in the EHA dynamics.
- They require an initial state-vector, prior error covariance, and noise statistics those can not always be known to control engineers.
- The complexity of the covariance matrices assumption increases with the number of states.
- Their estimation performance can be degraded under time-correlated noise.

Finite impulse response (FIR)-structured Kalman filtering and its application for fault estimation problem were successfully carried out in [28]. Here, by using a quadratic minimization scheme, an estimator was developed with necessary and sufficient conditions that could deal with the sensor fault problem with white-noise. However, it still requires the covariance-elements to minimize the cost function defined in Krein space. Though strong theoretical analysis proved its convergence for linear systems, it was not carried out for nonlinear dynamics where linearization error could affect the convergence process. Meanwhile, Ref. [29] recently proposed the extended finite impulse response (EFIR) filter. With $N$ recent past measurements, it can operate in Kalman-like recursion form and ensures robustness while overcoming the difficulties of existing filters such as estimation-divergence under 'non-white Gaussian' noise, high-sensitivity of noise statistics in state estimation, etc. [30]. Thus, it was carried out into many nonlinear applications successfully [31–33]. But, to the best of our knowledge, no study of the EFIR has been conducted in the sensor fault diagnosis field. Certainly, unlike the UIO, the current form of the EFIR cannot tolerate the unknown inputs. On the contrary, the existing UIO cannot handle the system-nonlinearities and noises as discussed before. Consequently, by integrating an UIO into the EFIR architecture, the unknown input decoupled stochastic-state estimation can be performed in the FIR manner. This allows us to overcome the above-mentioned flaws and generate robust-residuals under the faulty condition with minimum design-effort. Besides, the challenge of designing an effective sensor FTC framework that should work with any error-based control logic can be solved.

In this paper, we present a novel unknown input observer combined EFIR estimator (UIOEFIR) and apply for the sensor fault-tolerant tracking control of an EHA. The control-objective here is to maintain the EHA tracking stability under

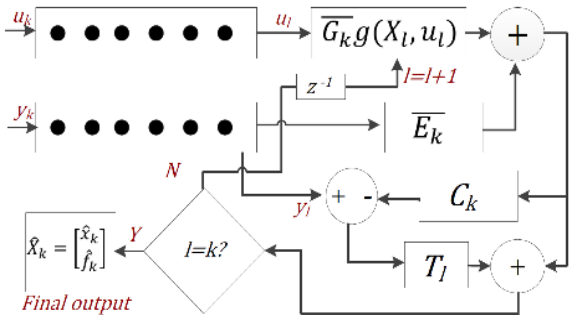


Figure 1: Schematic of the proposed UIOEFIR

different sensor-fault conditions using the UIOEFIR. Our contributions in this paper are summarized as: Firstly, unlike [29] and other observer-based fault diagnosis approaches presented in [8], [18] and [28], the newly developed UIOEFIR can simultaneously estimate the system states and the unknown fault magnitude without providing prior-noise-statistics whilst defining only single parameter $N$. Thus, the design complexity is significantly minimized. Secondly, by taking the nonlinearities and linearization error into account, we derive the estimator convergence condition using Lyapunov-stability-based analysis which was presumably overlooked in [28]. Thirdly, we incorporate the proposed estimator as a part of FDA, capable to work with any error-based controller. The technique is then employed for EHA sensor fault-tolerant tracking control. To this end, a numerical model of the EHA is developed and multiple UIOEFIRs are designed for different installed-sensors. Then the FTC for EHA is performed by evaluating robust-residuals evaluation and switching feedback signal from faulty to healthy estimation. Consequently, tracking stability retains. We investigate the performance of UIOEFIR with both simulation and real-time analysis under the optimal $N = N_{opt}$ and 50% downgrade setting of $N_{opt}$ respectively. Results are then compared with a very well designed EKF-based UIO (UIOEKF) with known noise statistics. Results show that, without providing any initial condition or covariance matrix, the proposed UIOEFIR is equally efficient as the near-accurately designed UIOEKF. Additionally, it shows more robustness and improves estimation accuracy while handling time-correlated noises under similar sensor fault conditions.

## II. Design Procedure of UIOEFIR Estimator

Assume a non-linear system with sensor observation is

$$\begin{aligned} x_k &= f(x_{k-1}, u_k) + W_k \\ y_k &= Zx_k + E^{j,i} d_k^{j,i} + V_k \end{aligned} \tag{1}$$

where $x_k \in \Re^K$, $u_k \in \Re^L$, and $y_k \in \Re^S$ are the state vector, control input and measurement vector at time-step $k$, respectively; the superscripts $K$, $L$ and $S$ are the number of states, control inputs and measurements; $f(.)$ is the nonlinear function; $Z$ is the output matrix; and $W_k$ and $V_k$ are the process and measurement noise vector, respectively. $d_k^{j,i} \in \Re$ is a scalar that denotes the evolution of the $i^{th}$ sensor fault at time-step $k$ and $E^{j,i} = [0 \ldots 1 \ldots 0]^T$ is a standard vector.

Standard Kalman-like filters are generally hampered when the fault affects to a sensor (i.e. $E[d_k^{j,i}] \neq 0$). Here, the UIO plays a significant role to tackle this problem. A general design proceedure of the UIO can be found in the supplementary document. Now, to design robust UIOEFIR, consider the sensor fault dynamics is expressed by (2) [25, 34]

$$d_k^{j,i} = d_{k-1}^{j,i} + \tau\xi_k + v_{i,k} \tag{2}$$

where $\tau$ is the sampling time, $\xi_k$ is the sensor error input and $v_{i,k} \in \Re$ represents noise during fault. From (1) and (2), the new system state space representation can be expressed as

$$\underbrace{\begin{bmatrix} x_k \\ d_k^{j,i} \end{bmatrix}}_{X_k} = \underbrace{\begin{bmatrix} f(x_{k-1}, u_k) \\ d_{k-1}^{j,i} \end{bmatrix}}_{g(X_{k-1},u_k)} + \underbrace{\begin{bmatrix} 0 \\ \tau \end{bmatrix}}_{E_k} \xi_k + \underbrace{\begin{bmatrix} W_k \\ v_{i,k} \end{bmatrix}}_{W_{a,k}}$$
$$y_k = \underbrace{[Z \quad E^{j,i}]}_{C_k} X_k + V_k$$

That is

$$X_k = g(X_{k-1}, u_k) + E_k\xi_k + W_{a,k} \tag{3}$$

$$y_k = C_k X_k + V_k \tag{4}$$

where $X_k \in \Re^{K+1}$ is the augmented state vector, $E_k$ is the $i^{th}$ fault distribution vector. $R_k \in \Re^{L\times L}$ and $Q_k \in \Re^{K+1\times K+1}$ are in turn the covariance matrices of measurement noise vector $V_k$ and augmented process noise vector $W_{a,k}$. It is interesting to see that by defining the fault dynamics (2), the sensor-fault estimation in (1) can be performed as a similar technique to the actuator-fault estimation with UIO manner [35, eq. (1)]. Now, since the UIOEFIR exploits EFIR architecture [29], it requires $N \approx N_{opt}$ measurements (*N* is the horizon length) at the beginning. The initial state $\tilde{X}_s$ for time-step $s$ where $s = m + K$; $m = k - N + 1$ are approximated as

$$\tilde{X}_s = \begin{cases} \begin{bmatrix} y_s & 0 \end{bmatrix}^T, \text{if } s < N-1 \\ \hat{X}_s, \text{if } s \geq N-1 \end{cases} \tag{5}$$

**Assumption 1:** There is no fault until $N$ time steps are elapsed (i.e. $E[d_k^{j,i}] = 0$ for $k < N$).

The generalized noise power gain (GNPG) $G_s$ can be initialized with $I_{(K+1)\times(K+1)}$ as there is a negligible noise reduction while $k < N$. Next, if $rank(C_kE_k) = rank(E_k)$ is satisfied the following UIO-style relations can be derived [15]

$$H_k = (C_kE_k)^+ = [(C_kE_k)^T C_kE_k]^{-1}(C_kE_k)^T \tag{6}$$

$$\bar{G} = I - E_kH_kC_k \tag{7}$$

$$\bar{E}_k = E_kH_k \tag{8}$$

Then for $l$ ranges from $m + K + 1$ to $k$, prior estimation $\tilde{X}_{l/l-1}^-$, the Jacobian $F_l$ and its extension $\bar{F}_l$, GNPG $G_l$, gain $T_l$, and the estimated states $\tilde{X}_l$ are derived from (9) to (13):

$$\tilde{X}_{l/l-1}^- = \bar{G}.g(\tilde{X}_{l-1}, u_l) + \bar{E}_k y_l \tag{9}$$

$$\bar{F}_l = \left.\frac{\partial \bar{g}(\cdot)}{\partial X}\right|_{X=\hat{X}_{l-1}} = \bar{G}\left.\frac{\partial g(\cdot)}{\partial X}\right|_{X=\hat{X}_{l-1}} = \bar{G}F_l \tag{10}$$

$$G_l = \left[{C_k}^T C_k + \left(\bar{F}_l G_{l-1} \bar{F}_l^T\right)^{-1}\right]^{-1} \tag{11}$$

$$T_l = G_l {C_k}^T \tag{12}$$

**Algorithm 1** The UIOEFIR estimator algorithm

**Input:** $y_k$, $K$, $N$
**while** $(k < N-1)$ SET $\hat{X}_k = [y_k\, 0]^T$, $Res_k = 0_{K\times 1}$
**while** $k \geq N-1$ **do**
  $H_k = (C_kE_k)^+ = [(C_kE_k)^T C_kE_k]^{-1}(C_kE_k)^T$
  $\bar{G} = I - E_kH_kC_k$; $\bar{E}_k = E_kH_k$
  $s = m + (K+1) - 1$; $m = k - N + 1$
  **set** $\tilde{X}_s = \begin{cases} [y_s\, 0]^T, \, if\, s < N-1 \\ \hat{X}_s, \, if\, s \geq N-1 \end{cases}$ and $G_s = I$
  **for** $l = m + K + 1$ to $k$ **do**
    $\tilde{X}_{l/l-1}^- = \bar{G}.g(\tilde{X}_{l-1}, u_l) + \bar{E}_k y_l$
    $G_l = \left[{C_k}^T C_k + \left(\bar{F}_l G_{l-1} \bar{F}_l^T\right)^{-1}\right]^{-1}$; $\bar{F}_l = \bar{G}F_l$
    $T_l = G_l {C_k}^T$
    $\tilde{X}_l = \tilde{X}_{l/l-1}^- + T_l(Res_l)$; $Res_l = (y_l - C_k\tilde{X}_{l/l-1}^-)$
  **end for**
  $\hat{X}_k = \tilde{X}_l$, $Res_k = Res_l$
  $k = k + 1$
**end while**
**Output:** $\hat{X}_k$, $Res_k$

$$\begin{aligned} \tilde{X}_l &= \tilde{X}_{l/l-1}^- + T_l(Res_l) \\ Res_l &= (y_l - C_k\tilde{X}_{l/l-1}^-) \end{aligned} \tag{13}$$

where, $Res_l$ is the residual matrix. Finally, compute the output $\hat{X}_k = \tilde{X}_l$ at $l = k$. *Algorithm 1* further summarizes the design procedure of UIOEFIR with a schematic in Figure 1.

### A. Convergence condition

Let the nonlinear system is expressed at point $l$ as:

$$\begin{aligned} X_l &= g(X_{l-1}, u_l) + E_l\xi_l \\ y_l &= C_kX_l + V_l \end{aligned} \tag{14}$$

From (13) and (14) the estimation error becomes $e_l = X_l - \tilde{X}_l = [I - T_lC]\, e_{l/l-1}$ where, $e_{l/l-1} = X_l - \tilde{X}_{l/l-1}^- \approx \bar{F}_{l-1}e_{l-1} = \alpha_{l-1}\bar{F}_{l-1}e_{l-1}$ with an unknown diagonal matrix $\alpha_{l-1} = diag(\alpha_{1,l-1}...\,\alpha_{n,l-1})$. Define $P_{l/l-1}$ and $P_l$ be the the prior state covariance matrix and state covariance matrix at point $l$ respectively. For iteration ranges from $l$ to $k$ with any initial value $\tilde{X}_s$, the estimation of UIOEFIR converges to suboptimal region under the following condition:

**Theorem 1.** *Given any variable $\varphi$ where $0 < \varphi < 1$, $\underline{\lambda}(.)$, $\bar{\lambda}(.)$ and $\kappa(.)$ denotes the minimum, the maximum eigenvalues and condition number of (.), respectively, if*

$$\bar{\lambda}(\alpha_{l-1}) \leqslant \left[\frac{(1-\varphi)}{\bar{\lambda}\left(\bar{F}_{l-1}\right)^2 \kappa(P_{l-1})}\right]^{\frac{1}{2}}$$

*then the proposed UIOEFIR is asymptotically convergent.*

*Proof.* From (6)-(8) and (10) we find the extension of Jacobian matrix:

$$\begin{aligned} \bar{F}_{l-1} &= \bar{G}F_{l-1} \\ &= [I - E_k[(C_kE_k)^T(C_kE_k)]^{-1}(C_kE_k)^T C_k]F_{l-1} \end{aligned}$$

Now, $rank\left(E_k[(C_kE_k)^T(C_kE_k)]^{-1}(C_kE_k)^TC_k\right) \leq \min\left(rank\left(E_k\right), rank\left(C_k\right)\right)$. As $\tau > 0$, $E_k$ in (3) is a non-zero vector, $\bar{F}_{l-1}$ becomes singular. From [28], we have:

$$\begin{aligned} P_{l/l-1} &= \bar{F}_{l-1}P_{l-1}\bar{F}_{l-1}^T + Q_{l-1} \\ P_l &= (I - T_lC_k)P_{l/l-1}(I - T_lC_k)^T + T_lR_lT_l^T \end{aligned}$$

Consider a Lyapunov candidate function

$$\begin{aligned} V_l &= e_l^T P_l^{-1} e_l \\ &= e_{l-1}^T \bar{F}_{l-1}^T \alpha_{l-1}[I - T_lC_k]^T P_l^{-1}\left[I - T_lC_k\right]\alpha_{l-1}\bar{F}_{l-1}e_{l-1} \end{aligned} \tag{15}$$

Let, $X = [I - T_lC_k]$. By binomial matrix inversion lemma

$$\begin{aligned} P_l^{-1} &= \left[X_lP_{l/l-1}X_l^T + T_lR_lT_l^T\right]^{-1} \\ &= X_l^{-T}P_{l/l-1}^{-1}X_l^{-1} - X_l^{-T}P_{l/l-1}^{-1}X_l^{-1} \\ &\quad \times\left[X_l^{-T}P_{l/l-1}^{-1}X_l^{-1} + T_l^{-T}R_l^{-1}T_l^{-1}\right]^{-1} \\ &\quad \times\left[X_l^{-T}P_{l/l-1}^{-1}X_l^{-1}\right] \end{aligned} \tag{16}$$

Next, by manipulating (16) and (15), we get

$$\begin{aligned} V_l = e_{l-1}^T\bar{F}_{l-1}^T\alpha_{l-1}\Bigg[P_{l/l-1}^{-1} - P_{l/l-1}^{-1}\Big[P_{l/l-1}^{-1} \\ + X_l^TT_l^{-T}R_l^{-1}T_l^{-1}X_l\Big]^{-1}P_{l/l-1}^{-1}\Bigg]\alpha_{l-1}\bar{F}_{l-1}e_{l-1} \end{aligned} \tag{17}$$

Now, using (12)

$$\begin{aligned} T_l^{-1} &= (G_l{C_k}^T)^{-1} \\ &= C_k + {C_k}^{-T}\left[\bar{F}_{l-1}G_{l-1}\bar{F}_{l-1}^T\right]^{-1} \\ T_l^{-1}X_l &= T_l^{-1}\left[I - T_lC_k\right] \\ &= {C_k}^{-T}\left[\bar{F}_{l-1}G_{l-1}\bar{F}_{l-1}^T\right]^{-1} \end{aligned} \tag{18}$$

From (17) and (18), we find

$$\begin{aligned} V_l = e_{l-1}^T\bar{F}_{l-1}^T\alpha_{l-1}\Bigg[P_{l/l-1}^{-1} - P_{l/l-1}^{-1}\Big[P_{l/l-1}^{-1} \\ + [\bar{F}_{l-1}G_{l-1}\bar{F}_{l-1}^T]^{-T}{C_k}^{-1}R_l^{-1}{C_k}^{-T} \\ \times\left[\bar{F}_{l-1}G_{l-1}\bar{F}_{l-1}^T\right]^{-1}\Big]^{-1}P_{l/l-1}^{-1}\Bigg]\alpha_{l-1}\bar{F}_{l-1}e_{l-1} \end{aligned} \tag{19}$$

And $V_{l-1} = e_{l-1}^TP_{l-1}^{-1}e_{l-1}$. If $\varphi$; $0 < \varphi < 1$, be the parameter subject to the exponential convergence rate [36] then the condition $V_l - (1-\varphi)V_{l-1} \leq 0$ must be satisfied. By inserting the values of $V_l$ and $V_{l-1}$, we obtain

$$\begin{aligned} e_{l-1}^T\Bigg(\bar{F}_{l-1}^T\alpha_{l-1}P_{l/l-1}^{-1}\alpha_{l-1}\bar{F}_{l-1} - \bar{F}_{l-1}^T\alpha_{l-1}P_{l/l-1}^{-1} \\ \times\Bigg[P_{l/l-1}^{-1} + \left[\bar{F}_{l-1}G_{l-1}\bar{F}_{l-1}^T\right]^{-T}{C_k}^{-1}R_l^{-1}{C_k}^{-T} \\ \times\left[\bar{F}_{l-1}G_{l-1}\bar{F}_{l-1}^T\right]^{-1}\Bigg]^{-1}P_{l/l-1}^{-1}\alpha_{l-1}\bar{F}_{l-1} \\ -(1-\varphi)P_{l-1}^{-1}\Bigg)e_{l-1} \leq 0 \end{aligned} \tag{20}$$

The inequality of the Rayleigh quotient for $\Lambda \geq 0$ is expressed as $\underline{\lambda}(\Lambda) \leqslant \frac{e_{l-1}^T\Lambda e_{l-1}}{e_{l-1}^Te_{l-1}} \leqslant \bar{\lambda}(\Lambda)$ and therefore

$$\begin{aligned} \bar{\lambda}\left(\bar{F}_{l-1}^T\alpha_{l-1}P_{l/l-1}^{-1}\alpha_{l-1}\bar{F}_{l-1}\right) - \underline{\lambda}\Big(\bar{F}_{l-1}^T\alpha_{l-1}P_{l/l-1}^{-1} \\ \times\Big[P_{l/l-1}^{-1} + \left[\bar{F}_{l-1}G_{l-1}\bar{F}_{l-1}^T\right]^{-T}{C_k}^{-1}R_l^{-1}{C_k}^{-T} \\ \times\left[\bar{F}_{l-1}G_{l-1}\bar{F}_{l-1}^T\right]^{-1}\Big]^{-1}P_{l/l-1}^{-1}\alpha_{l-1}\bar{F}_{l-1}\Big) \\ -(1-\varphi)\underline{\lambda}\left(P_{l-1}^{-1}\right) \leqslant 0 \end{aligned} \tag{21}$$

Now, since $\bar{F}_{l-1}$ is a singular matrix, $\underline{\lambda}\big(\bar{F}_{l-1}\big) = 0$; and $Q_{l-1}$ is a positive definite. So using the Weyl's inequality, $\underline{\lambda}\big(P_{l/l-1}\big) \leqslant \underline{\lambda}\big(\bar{P}_{l-1}\big)$ and from (21), the positive part:

$$\bar{\lambda}\left(\bar{F}_{l-1}^T\alpha_{l-1}P_{l/l-1}^{-1}\alpha_{l-1}\bar{F}_{l-1}\right) \leqslant \bar{\lambda}(\alpha_{l-1})^2\bar{\lambda}\big(\bar{F}_{l-1}\big)^2\underline{\lambda}(P_{l-1})^{-1}$$

And the negative part:

$$\begin{aligned} \underline{\lambda}(...) \geqslant \underline{\lambda}(\alpha_{l-1})^2\underline{\lambda}\big(\bar{F}_{l-1}\big)^2\underline{\lambda}\Big(P_{l/l-1}^{-1}\Big)^2\underline{\lambda}\Bigg(\Big[P_{l/l-1}^{-1} + \\ \left[\bar{F}_{l-1}G_{l-1}\bar{F}_{l-1}^T\right]^{-T}{C_k}^{-1}R_l^{-1}{C_k}^{-T}\left[\bar{F}_{l-1}G_{l-1}\bar{F}_{l-1}^T\right]^{-1}\Big]^{-1}\Bigg) \end{aligned}$$

Therefore, (21) becomes

$$\begin{aligned} &\bar{\lambda}(\alpha_{l-1})^2\bar{\lambda}\big(\bar{F}_{l-1}\big)^2\underline{\lambda}(P_{l-1})^{-1} \\ &\leqslant \frac{\underline{\lambda}(\alpha_{l-1})^2\underline{\lambda}\big(\bar{F}_{l-1}\big)^2\underline{\lambda}\Big(P_{l/l-1}^{-1}\Big)^2\underline{\lambda}(C_k)^2}{\underline{\lambda}(C_k)^2\bar{\lambda}\Big(P_{l/l-1}^{-1}\Big)+\bar{\lambda}\Big([\bar{F}_{l-1}G_{l-1}\bar{F}_{l-1}^T]^{-1}\Big)^2\bar{\lambda}\left(R_l^{-1}\right)} \\ &+(1-\varphi)\underline{\lambda}\left(P_{l-1}^{-1}\right) \end{aligned} \tag{22}$$

Let $\kappa(P_{l-1}) = \bar{\lambda}(P_{l-1})/\underline{\lambda}(P_{l-1})$ and putting $\underline{\lambda}\big(\bar{F}_{l-1}\big) = 0$

$$\bar{\lambda}(\alpha_{l-1}) \leqslant \left[\frac{(1-\varphi)}{\bar{\lambda}\big(\bar{F}_{l-1}\big)^2\kappa(P_{l-1})}\right]^{\frac{1}{2}} \tag{23}$$

And proves Theorem 1. □

***Remark 1***: In contrast to the previous works [16] and [28], where convergence were studied with the expectation of fixed variences or output quantization errors, this paper investigates the boundary of linearization error for any nonlinear systems while designing the sensor fault estimator.

## III. Applying UIOEFIR in Sensor fault-tolerant Tracking Control

Technically, a sensor FTC should act as a conventional closed-loop control logic. Under the no-fault condition, the sensor fault detection, isolation, and identification should be performed successively if any fault appears. Finally, control-logic reconfiguration is needed to maintain overall stability. Here, a simple sensor FTC architecture is realized in Figure. 2. A bank of UIOEFIRs monitors the plant outputs and performs state estimations. Next, based on their residual evaluation, healthy estimations and proper fault signal are classified by the sensor fault detection and isolation (FDI). Later, reconfiguration is performed by switching between stabilizing controllers [37]. The sensor FDI and the tracking-error-generation modules then generate the reconfigurable tracking error $e^*$

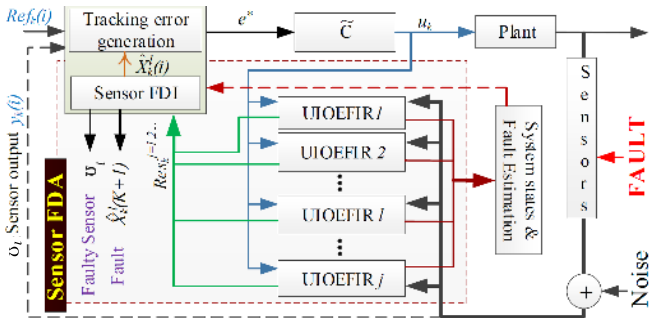


Figure 2: Sensor FTC for the EHA system

and feed to the controller $\widetilde{C}$. Next, the controller performs trajectory tracking according to the reference provided. The $e^*$ calculation and sensor FDI design steps are summerised as follows:

*i) Fault detection and isolation:* Firstly, using *Algorithm 1*, $\aleph$ UIOEFIRs; $\aleph \in \{1, 2, ...l, ...j\}$ are developed for the system (1) with $\{\mho_1, \mho_2, ...\mho_i\}$ sensors. Then, the $j^{th}$ UIOEFIR estimates the state $\hat{X}_k^j$ and generates the residual vector $Res_k^j(i)$ at time step $k$. Now, define

$$\begin{aligned} \beta_r = 0 \ ; \ r \in \aleph \backslash \{\ell\} \\ \beta_\ell = 1 \ ; \ \ell = \{j \in \aleph | \ -\epsilon_j(i) < Res_k^j(i) < \epsilon_j(i)\} \end{aligned} \tag{24}$$

here $\{\ell\}$ is a set of healthy UIOEFIR estimators and there exist no sensor faults when $\{\ell\} = \aleph$ satisfies. The sensor $\mho_\ell$ can be announced faulty when all of the associated residual-elements exceed the threshold $|\epsilon_j(i)|$ except for the estimator $j \in \{\ell\}$. Here $\epsilon_j(i)$ is calculated as: Let, $\sigma_j^2(i)$ is the $i^{th}$ residual-variance from $j^{th}$ observer. So, in fault free condition, we calculate the residual mean $r_j(i) = E[Res_k^j(i)] = 1/N \sum_{h=1}^{N} Res_h^j(i)$ and $\sigma_j^2(i) = 1/N \sum_{h=1}^{N} (Res_h^j(i) - r_j(i))^2$. Finally, $\epsilon_j(i) = (r_j(i) + \eta(i)\sigma_j(i))$, where $\eta(i)$ is the tolerance parameter subjected to the uncertainty boundary of the system. This value can be obtained by a simple characterisation test on the system when it is stationary.

*ii) Error signal generation:* The sensor FDI and the control error generation module takes $y_k(i)$ from the tracking sensor $\mho_i$ and $Res_k^j$. We define the $i^{th}$ state tracking error and associated estimator tracking error as (25).

$$e_a = y_k(i) - Ref_k(i); \quad \hat{e}_j = \hat{X}_k^j(i) - Ref_k(i) \tag{25}$$

where $Ref_k(i)$ is the tracking reference signal for closed-loop controller. At "no-fault" condition, error $e^* = e_a$ should be maintained for conventional tracking operation. Once $\mho_l$ sensor becomes faulty, $e^*$ is reconfigured and obtained by average healthy estimates: $e^* = \frac{\sum_{p=1}^{j} \beta_p \hat{e}_j}{\sum_{p=1}^{j} \beta_p}$. *Algorithm 2* then summarizes the decision of the sensor FDI and $e^*$ generation principle. It is noted that in case of all-sensors failure condition, no healthy estimation would exist ($\ell = \{\phi\}$) because all of the estimator- residuals exceed the pre-set thresholds. Consequently, emergency-stop decision is made for further protection. Based on the modified tracking error definition, controller $\widetilde{C}$ then generates the control effort $u_k \in \{\Gamma(e_a), \Gamma(e_j)\}$ with the following assumption.

**Algorithm 2** Sensor FDI & effective tracking error generation

**Define**, (24)
**if** $\{\ell\} = \aleph$ **then**
  decision: *No fault occurred*
  set $e^* = e_a = y_k(i) - Ref_k(i)$
**else if** $\{\ell\} \neq \aleph$ and $\{\ell\} \subset \aleph$ **then**
  decision: (a) *fault is detected at* $\mho_\ell$ *sensor* (b) Associated estimate is $\hat{X}_k^\ell$ from $\ell^t h$ UIOEFIR estimator
  set $e^* = \frac{\sum_{p=1}^{j} \beta_p \hat{e}_j}{\sum_{p=1}^{j} \beta_p}$
**else**
  decision: emergency stop (for $\ell = \{\phi\}$)
  set $e^* = 0$, or $\Gamma(e_a) = 0$
**end if**
**Output:** $e^*$, decision

***Assumption 3:*** The LTI controller $\widetilde{C}$ is at least an asymptotic stable for error input $e_a$ under no-fault condition (i.e. $\Gamma(e_a)$ is stable for $d_k^{j,i} = 0$)

***Remark 2*** *(Stability in FTC)*: When sensor FDA incorporates, switching of control efforts takes place and the overall closed loop stability then depends on: (i) Stability of $\Gamma(e_a)$, (ii)Stability of $\Gamma(e_j)$, and (iii) Stability within switching period. One can satisfy (i) by developing Lyapunov-based conventional controller, where (ii) is completely depended on the convergence condition of UIOEFIR estimation studied in Section II. Lastly, (iii) can be ensured by introducing a reset map and without the loss of generality, it can be assumed linear when the system has low natural frequency and the switching time is sufficiently small [38, 39]. Now, when a fault $d_k^{j,i}$ appears in $i^{th}$ sensor at time step $k$, $u^*(k)$ does not rely on $e_a$ anymore but $e_j(k)$ and hence, the effect of $d_k^{j,i}$ diminished.

## IV. Sensor FTC for an EHA

### A. Dynamic modeling of an EHA system

Generally, in the EHA (Figure 3a), a motor controls the bi-directional pump with displacement $D$ at rotational speed $\omega$ and draws $Q_{pump} = D\omega$ flow per unit time. Hence, the head-side pressure $P_h$ in chamber $Ch_h$ and the rod-side pressure $P_r$ in chamber $Ch_r$ are developed. Consequently, the cylinder piston **P** with equivalent mass $m_c$ moves to its position $x_p$ and experiences the friction force $fr$. The volumes of chamber $Ch_h$ and $Ch_r$ are calculated as $V^*{}_h = V_{ch} + x_p A_h$ and $V^*{}_r = V_{cr} + (l_c - x_p)A_r$ respectively. Here, $A_r$, $A_h$, $V_{ch}$ and $V_{cr}$ are in turn the head and rod-side areas of the piston **P** and the constant pipe volumes of $Ch_h$ and $Ch_r$. The hydraulic circuit has been illustrated in Figure 3b. Here, two pilot-operated check valves $v_1$ and $v_2$ are placed in a way that, their pilot-pressure lines are connected to $Ch_r$ and $Ch_h$ chambers respectively. That is, the pilot pressures $l_{px}$ and $r_{px}$ of valves $v_1$ and $v_2$ are set as $l_{px} = P_r$ and $r_{px} = P_h$. The opening areas of $v_1$ and $v_2$ valves $lA_p$ and $rA_p$ reach to their maximum $A_{p_{\max}}$ independently when their corresponding activation pressure $lP_e$(for $v_1$) or $rP_e$(for $v_2$) exceeds pre-set cracking-pressure $P_{crack} = 1.5$ bar. Otherwise, $lA_p = A_{pleak}$ or $rA_p = A_{pleak}$ ($A_{pleak}$ is the leaking area) can be set at the

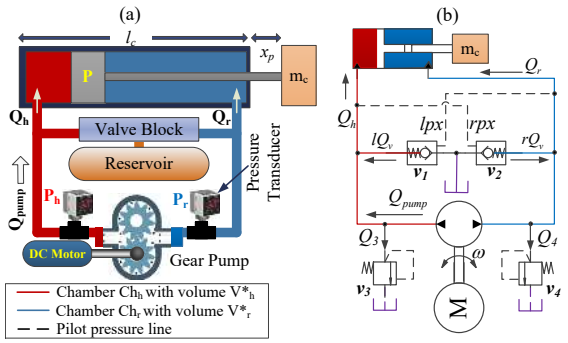


Figure 3: a) Electro hydraulic Actuator (b) Hydraulic circuit of an EHA

closing state of any valves. Hence, fluid enters into the circuit with flow rate $lQ_v$ and $rQ_v$ through $lA_p$ and $rA_p$ respectively. The relief valves $v_3$ and $v_4$ allow the leakage of excess fluid inside the circuit $Q_3$ and $Q_4$. Finally, per unit time, $Q_h$ and $Q_r$ flow enter/exit into/from the cylinder. So, $Q_h$, $Q_r$, $lQ_v$, $rQ_v$ can be formulated as [38]

$$\begin{aligned} Q_h &= Q_{pump} + lQ_v - Q_3 \\ Q_r &= -Q_{pump} + rQ_v - Q_4 \\ lA_p &= \begin{cases} A_{p\max}, & if\ lP_e > P_{crack} \\ A_{pleak}, & otherwise \end{cases} \\ rA_p &= \begin{cases} A_{p\max}, & if\ rP_e > P_{crack} \\ A_{pleak}, & otherwise \end{cases} \end{aligned} \tag{26}$$

$$\begin{aligned} lP_e &= lpx * kp_c - P_h \\ rP_e &= rpx * kp_c - P_r \\ lQ_v &= C_{dl} * lA_p * \sqrt{\tfrac{2\,abs(P_h)}{\rho}} sign(-P_h) \\ rQ_v &= C_{dr} * rA_p * \sqrt{\tfrac{2\,abs(P_r)}{\rho}} sign(-P_r) \end{aligned} \tag{27}$$

here $kp_c$, $C_{dl}$ and $C_{dr}$ are the valve constants and discharge coefficients, respectively. If $E_{max}$ is the bulk modulus of hydraulic fluid, and the effective bulk moduli: $\beta_{ch}$ and $\beta_{cr}$ then the continuity equations of fluid flow are expressed as

$$\begin{aligned} \beta_{ch} &= E_{\max}(1 - e^{(0.4-2\times10^7 P_h)}) \\ \beta_{cr} &= E_{\max}(1 - e^{(0.4-2\times10^7 P_r)}) \\ \tfrac{dP_h}{dt} &= \tfrac{\beta_{ch}}{V_{ch}+x_p A_h}(Q_h - \dot{x}_p A_h) \\ \tfrac{dP_r}{dt} &= \tfrac{\beta_{cr}}{V_{cr}+(l_c-x_p)A_r}(Q_r + \dot{x}_p A_r) \end{aligned} \tag{28}$$

Now, the dynamics of the piston can be described as

$$m_c\ddot{x}_p = (A_h P_h - A_r P_r) - fr; fr = \begin{cases} v_{f1}\dot{x}_p; \dot{x}_p > 0 \\ v_{f2}\dot{x}_p; else \end{cases} \tag{29}$$

From (26) to (29), the system state vector $X = \begin{bmatrix} x_1 & x_2 & x_3 & x_4 \end{bmatrix}^T = \begin{bmatrix} \dot{x}_p & x_p & P_h & P_r \end{bmatrix}^T$ is as (30)

$$\dot{X} = \begin{bmatrix} \dot{x}_1 \\ \dot{x}_2 \\ \dot{x}_3 \\ \dot{x}_4 \end{bmatrix} = \begin{bmatrix} \frac{1}{m_c}(A_h x_3 - A_r x_4 - fr) \\ x_1 \\ \frac{\beta_{ch}}{V_{ch}+x_2 A_h}(Q_h - x_1 A_h) \\ \frac{\beta_{cr}}{V_{cr}+(l_c-x_2)A_r}(Q_r + x_1 A_r) \end{bmatrix} \tag{30}$$

Table I: EHA parameters

| Parameters | Values |
|---|---|
| Piston areas $A_h$, $A_R$ | 4.91 $cm^2$, 3.76$cm^2$ |
| Opening/leaking areas $A_{pmax}/A_{pleak}$ | 7.686$mm^2$/10$^{-6}mm^2$ |
| Bulk modulus of the hydraulic fluid $E_{max}$ | $1.8 \times 10^9 Pa$ |
| Cylinder length $l_c$ | $150mm$ |
| Piston mass $m_c$ | $0.5kg$ |
| Hydraulic fluid density $\rho$ | $870Kg/m^3$ |
| Valve coefficients $C_{dl}$, $C_{dr}$ | 0.6 |
| Friction parameters $v_{f1}$, $v_{f2}$ | 600, 580 |
| Valve constant $kp_c$ | 1.8 |
| Constant Chamber volume $V_{ch}$, $V_{cr}$ | 0.1 $L$ |
| Pump displacement $D$ | 1.7 $cc$ |

(30) can be further discritized using Taylor $1^{st}$ order approximation: $X_k \approx X_{k-1} + \tau\dot{X}$. Considering the linearization error, the EHA dynamics can be finally realized as

$$\begin{aligned} X_k &= g(X_{k-1}, u_k) + \tau\dot{X} \\ Y_k &= ZX_k \end{aligned} \tag{31}$$

where $u_k = \omega$ is control input, and $Y_k$, $g(.)$, $Z$, $W_k$, $V_k$, $E^{s,i}$ and $d_k^{s,i}$ have their usual meanings (See Section II).

### B. Design Procedure of Sensor FTC

A multi-sensor fault-tolerant tracking control is developed using *Algorithms 1* and *2*. Here, sensor-faults in the head-side pressure ($P_h$) and position ($x_p$) sensors of the EHA are considered to examine the UIOEFIR estimator performance. The remainder of the sensors and actuator are assumed to not be faulty. The target is to perform a position tracking control task of the EHA in faulty conditions and evaluate the estimation performance. Although the pressure fault does not directly affect the position control performance, it can influence the system safety. Therefore, the sensor FDA should classify this fault and set an alarm to ensure safe operation. The design steps of the sensor FTC scheme for EHA are:

*Step 1:* The EHA is realized by (31) using the parameters listed in Table I, and extended as (3) using fault model (2). Since the number of states $K = 4$, $E_k$ in (3) becomes $E_k = \begin{bmatrix} 0 & 0 & 0 & \tau \end{bmatrix}^T; \forall\tau > 0$. Hence, the state vector $X_k$ and nonlinear function $g(X_{k-1}, u_k)$ in (2) are obtained.

*Step 2:* Using *Algorithm 1*, two UIOEFIR estimators: UIOEFIR_pos (for the $x_p$ position sensor) and UIOEFIR_pr (for the $P_h$ pressure sensor) are developed by setting $C_K(pos) = \begin{bmatrix} Z & E^{pos,i} \end{bmatrix}^T$ and $C_K(pr) = \begin{bmatrix} Z & E^{pr,i} \end{bmatrix}^T$, respectively. Where sensor selection vectors: $E^{pr,i} = \begin{bmatrix} 0 & 0 & 1 & 0 \end{bmatrix}^T$, $E^{pos,i} = \begin{bmatrix} 0 & 1 & 0 & 0 \end{bmatrix}^T$ and $Z = I_{K\times K}$.

*Step 3:* To find the optimal horizon length $N_{opt}$, the developed UIOEFIRs with EHA are run using different $N$ under fault free condition. Then, $N_{opt} = 50$ is found (Figure. 4) which minimizes the integrated-squared-error cost function,

$$ISE = \int trace(E_{est}E_{est}^T)dt \tag{32}$$

here $E_{est} = (x_k - \hat{x}_k)$ is the estimation error vector. Next, the estimated system states $\hat{X}_k^s$ and the residual vector $Res_k^s$ can be obtained from the corresponding estimator '$s$'; $s \in \{UIOEFIR\_pos, UIOEFIR\_pr\}$.

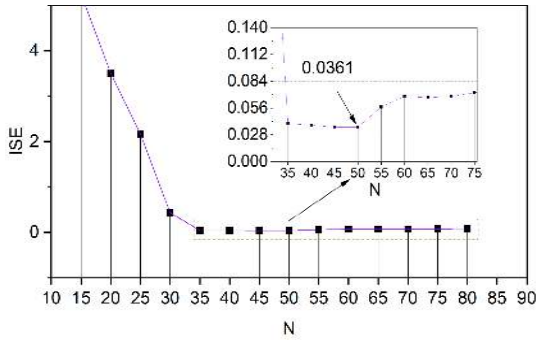


Figure 4: Selection of optimal horizon length $N_{opt}$ by cost function evaluation with respect to different horizon size

*step 4:* Finally, a sensor FTC with FDI process are realized by Figure 2 and Algorithm 2. In this paper, a simple PID controller ($K_p = 25$, $K_i = 2.3$, $K_d = 0.02$) is optimized using a local search algorithm. The position and $P_h$ pressure residual thresholds in (27) are carefully set as $\varepsilon_{pos}(2) = \pm 0.015m$ and $\varepsilon_{pr}(3) = \pm 5bar$. These parameters can be set by trial-and-error method or by engaging other optimization algorithms.

## V. Performance Analysis and Case Studies

The proposed estimators and the sensor FTC architecture were designed and evaluated in Matlab/Simulink environment with the sampling time: $\tau = 0.001$s. Results are compared with the well-known unknown-input-observer embedded extended Kalman filter (UIOEKF) [25,26]. Similar sensor FTC architecture was retained by designing the estimators: UIOEKF_pos and UIOEKF_pr. For these estimators, it was assumed that all initial states were known almost exactly. Thus, the process, the measurement noise statistics and the prior estimation covariance matrix were set as:

$$P_k^{EKF} = diag\left(\begin{bmatrix} 10^{-8} & 10^{-8} & 10^{-8} & 10^{-8} & 0 \end{bmatrix}\right)$$
$$R_k = diag\left(\begin{bmatrix} 0.005^2 & 0.005^2 & 0.7^2 & 0.7^2 \end{bmatrix}\right)$$
$$Q_k = diag\left(\begin{bmatrix} 10^{-12} & 10^{-12} & 10^{-5} & 10^{-5} & 10^{20} \end{bmatrix}\right)$$

### A. Numerical simulations

*1) Case study 1:* Firstly, the fault in head-side pressure sensor was considered in the simulation. Figure. 5 shows that a typical trajectory tracking was performed, until the fault was invoked in the head-side pressure ($P_h$) sensor with $flt_{pr} = 150$ and $flt_{pr} = 300$ bar at $t = 25$s, and $t = 35$s, respectively (Figure 5a and 5b). Figure 5c suggests that both UIOEFIR_pr and UIOEKF_pr estimated the fault accurately. Next, by evaluating estimator-residuals, *Algorithm 2* could isolate the fault in $P_h$ sensor from the fault in $x_p$ sensor (Figure 5d and 5e). Thus, the alarm was set and the tracking continued. The state estimation performance of the UIOEFIR_pr and the UIOEKF_pr is compared in Figure. 6. As seen, the estimation of velocity (Figure 6a), position (Figure 6b), head-side pressure (Figure 6c) and rod-side pressure (Figure 6d) states for the UIOEFIR_pr, and the UIOEKF_pr were almost similar.

***Remark 3:*** It can be suggested that, when $N = N_{opt}$, the UIOEFIR is equally efficient as a near-perfect UIOEKF under

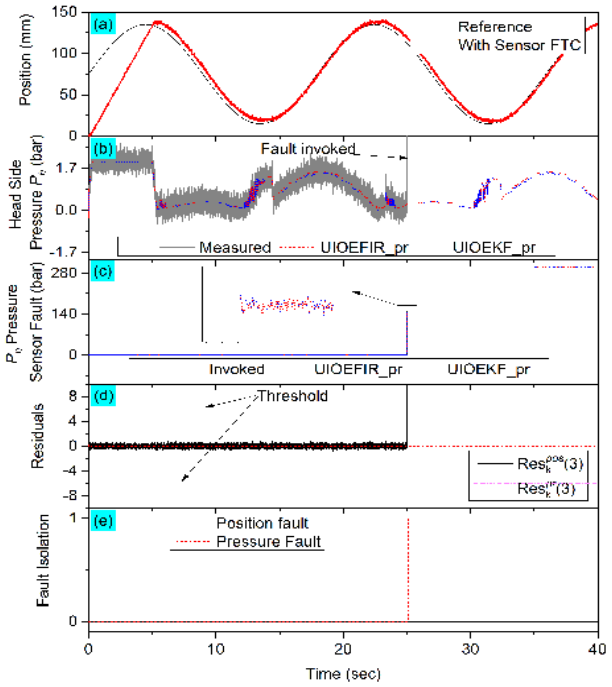


Figure 5: Pressure sensor fault scenarios and FTC performance

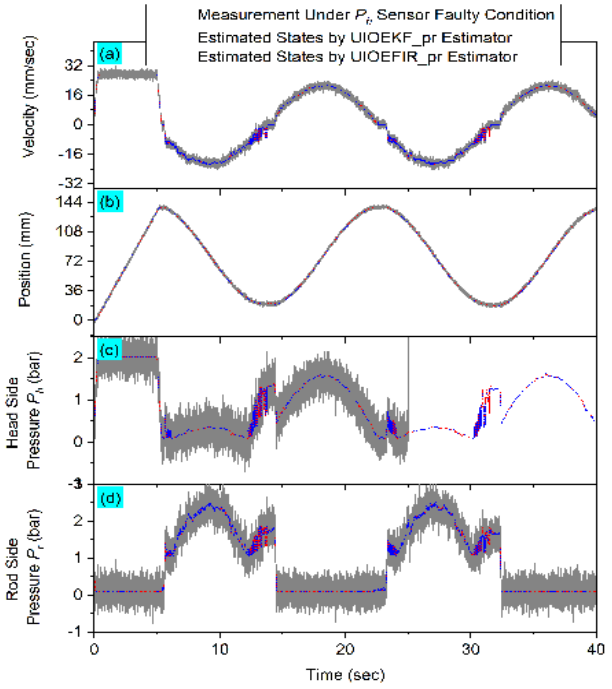


Figure 6: State estimation comparison of the UIOEFIR_pr and UIOEKF_pr under a fault in $P_h$ pressure sensor

sensor fault condition. Nevertheless, it is worth finding a single optimized value rather than matrices with high dimensionality. Next, we examine the performance when $N$ is sup-optimal.

*2) Case study 2:* The performance under position sensor fault was considered in this case study. Moreover, in order to investigate how the estimator handles time-correlated noise (developed by a noise generation program and added with

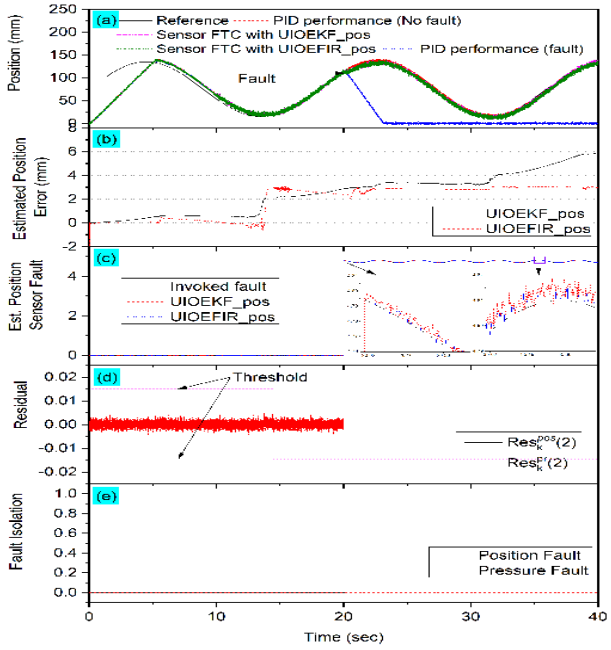


Figure 7: Position sensor fault and FTC performance

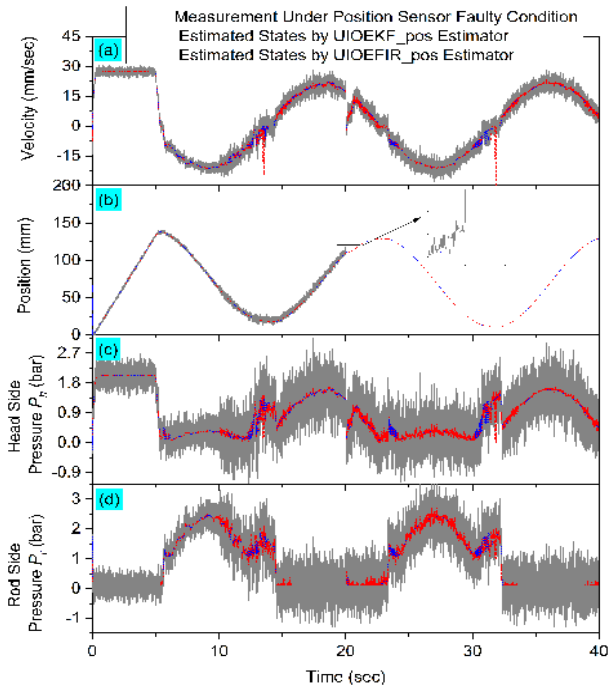


Figure 8: State estimation comparison of the UIOEFIR_pos and UIOEKF_pos under position sensor fault condition

the measurement vector), the noise level was increased by 100% at $t = 10$s. Figure. 7a shows that without having any sensor fault, the controller could perform the control objective. However, at $t = 20$s, the time-varying additive sensor fault $flt_{pos} = 4.75 + 0.06sin(\omega_2 t)$ with $\omega_2 = 2$ rad/sec was invoked in the position sensor which made the system unstable while the stability was retained using sensor FTC scheme. Figure. 7b clearly shows that compared to the UIOEFIR_pos,

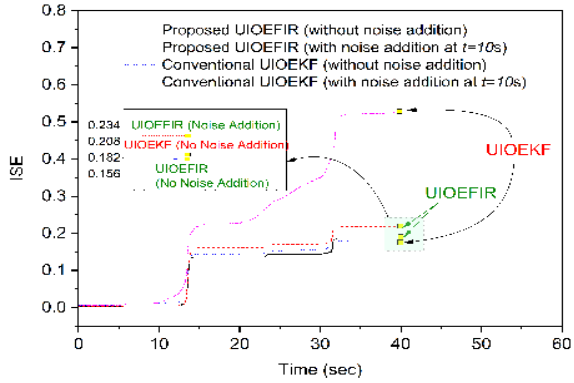


Figure 9: Effect of time-correlated noise on estimation-errors

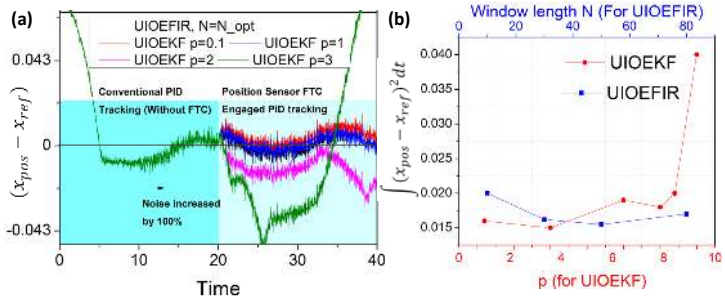


Figure 10: **a)** Tracking error performance of UIOEKF as function of $p$ in $p^2 Q_k$ and $R_k/p^2$. **b)** error cost representation for different $p$ (UIOEKF) and $N$ (UIOEFIR)

the UIOEKF_pos provided less-accurate position estimation performance. However, both of the estimators estimated the time-varying fault with acceptable performance (Figure. 7c). Next, Algorithm 2 evaluates the residual elements $Res_k^{pos}(2)$ and $Res_k^{pr}(2)$ of UIOEFIR_pos and UIOEFIR_pr, and ensured the position sensor fault condition (Figure. 7d and 7e). Finally, recovery was performed based on this decision.

The overall comparative studies of the UIOEFIR_pos and the UIOEKF_pos under position sensor fault condition are presented in Figure. 8. The two estimators provided almost identical performances until the noise levels were increased at $t = 10$s. However, unlike UIOEKF_pos, the estimation of the velocity (Figure. 8a), position (Figure. 8b), head-side pressure (Figure. 8c) and the rod-side pressure (Figure. 8d) states were not much affected for the UIOEFIR_pos.

***Remark 4:*** The sudden increment of the noise affected $Q$ and $R$ matrices of the UIOEKF. Meanwhile, optimal $N = 50$ of the UIOEFIR automatically becomes sub-optimal. Considering the ISE in (32), we run the process with and without noise addition under a similar sensor fault condition. Figure. 9 shows that the UIOEFIR's ISE (32) increases from 0.186 to 0.21 due to the effect of noise addition (16.5%). Meanwhile, for the EKF-based UIO, this cost increases from 0.18 to 0.531 (arround 195%). Hence, we conclude that, though the UIOEFIR is almost accurate to the UIOEKF (with known covariances and prior knowledge), it has shown robustness while handling time-correlated noises and similar sensor fault.

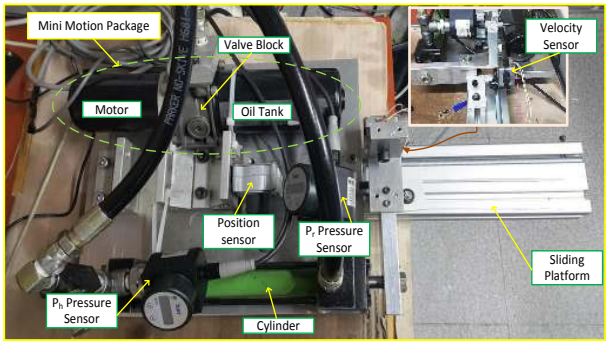


Figure 11: Experimental setup with EHA

*3) Case study 3:* Here we investigate the same scenario of *case study 2* but the $Q_k$ and $R_k$ of the UIOEKFs are not accurately known. To vary these accurately set matrices, a coefficient $p$ was introduced and substituted with $p^2Q_k$ and $R_k/p^2$. Figure 10 shows what went on with the tracking error and the error cost $\int (x_{pos} - x_{ref})^2 dt$ for different $p$. Figure 10a shows that the $p$ invariant UIOEFIR-based sensor FTC provided better tracking accuracy with $N_{opt} = 50$ while the UIOEKF-based FTC tracking performance varied with different $p$. Note that for inaccurate setting of $P_0$ may results larger tracking error. From Figure 10b, we can clearly say that, the tracking error cost $\int (x_{pos} - x_{ref})^2 dt$ for the UIOEFIR-based FTC did not vary significantly with different $N$ (solid-blue) as observed for the UIOEKF-based FTC with inaccurate co-variance matrix-configurations (solid-red). Due to the space limitation, multi-sensor FTC using the UIOEFIR has been investigated in the supplementary document (Section B).

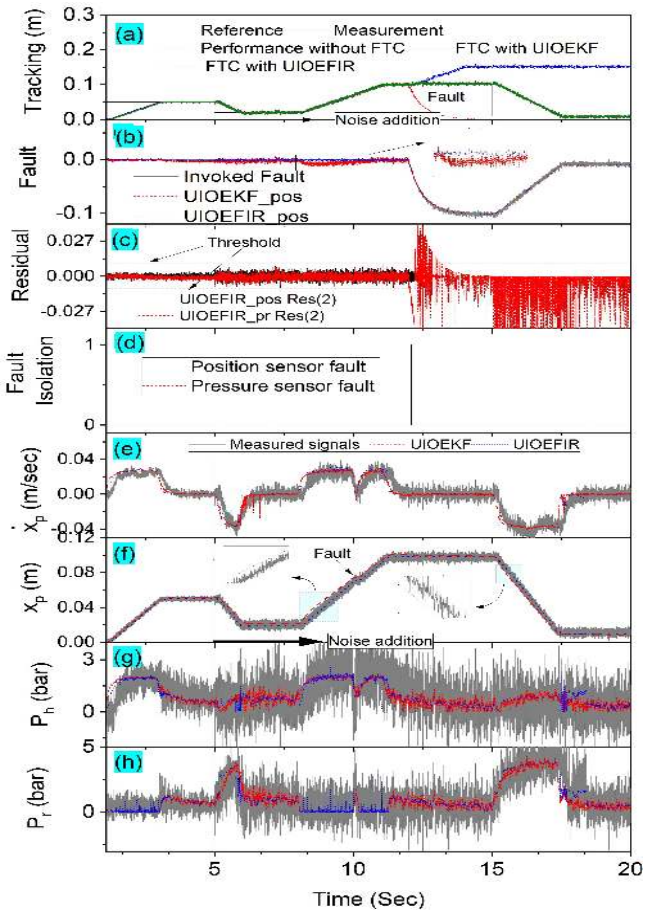


Figure 12: Sensor FTC and estimation performance with the position sensor fault condition

## VI. Experimental validation

The developed UIOEFIR-based real-time sensor FTC was carried out for an EHA presented in Figure. 11. This was a compact setup of a DC-motor, a gear pump, and hydraulic valve blocks having similar dynamic behaviours studied previously. The complete program was carried out by using the Matlab/Simulink Real-time toolbox in a PC with 2.9GHz - Core i5 and 2GB RAM, and NI 6221 Multifunction card from National Instruments (USA). The sampling time was $0.001s$ and the UIOEFIR horizon length was set to 50% of its optimal point ($N = 25$). The performance was then compared with the UIOEKF while performing with the presented FTC scheme. Moreover, to create a more challenging environment, all noise levels were increased by 100% from $t = 5$s. Similar to simulation cases, fault scenarios for both $x_p$ position sensor and $P_h$ pressure sensor-fault were studied.

*Experiment Case 1:* Firstly, a complete failure of position sensor is considered. As seen in Figure 12a, the position-feedback was exponentially set to zero (complete failure) between $12s$ and $15s$ (red-dash line). Consequently, the controller generated false-effort and but could not retain stability (blue-dot line) until any of the sensor FTCs was engaged (green dot-dash-line). Here, the fault estimation was noticeably better for the UIOEFIR_pos than the UIOEKF_pos (Figure. 12b). Figure 12c shows that Until $t = 12$s, position-residuals for the UIOEFIR_pos and the UIOEFIR_pr were within the defined threshold level $\varepsilon_{pos}(2) = \pm 0.015m$. When the fault was invoked the position residual of UIOEFIR_pos did not cross the pre-set threshold as observed for the UIOEFIR_pr. This suggested that the fault occurred in $x_p$ position sensor and the position-sensor-fault flag was set as 1 (Figure 12d). At this point, *Algorithm 2* re-defined the control error by switching the feedback from faulty measurement to the healthy estimation of the UIOEFIR_pos and consequently, the closed-loop stability was retained. A supplementary video can be downloaded from here. A comparative states estimation performance can be depicted in the figure. 12 (a-h). The estimations performed by both of the estimators were found almost identical until $t = 5$s. After this time-period, the noise levels were increased and the estimated velocity of UIOEKF_pos was slightly disturbed due to its high sensitivity. However acceptable estimation was obtained by the designed method (Figure. 12(e)). In addition, compare to the UIOEKF_pos, UIOEFIR_pos estimated the position state of the EHA accurately (Figure. 12f). Moreover, head and rod-side pressure estimations were performed comparatively better by UIOEFIR (Figure. 12g and 12h). Clearly, even at below-optimal setting ($N = 25$), the UIOEFIR_pos effectively handles the time-correlated noises compared to the UIOEKF_pos under similar fault conditions.

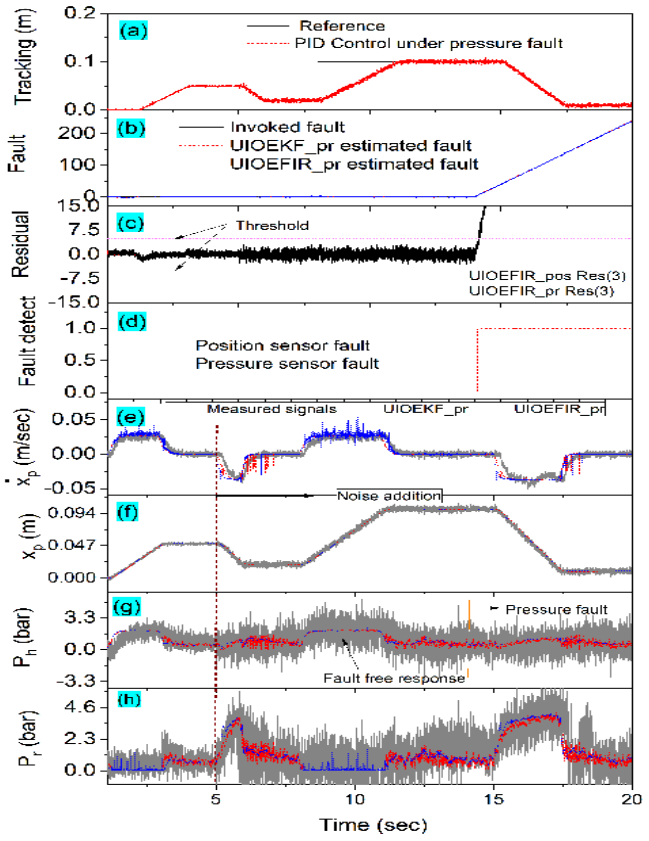


Figure 13: Sensor FTC and estimation performances with the fault in $P_h$ pressure sensor

*Experimental Case 2:* In this case study, fault in pressure sensor is considered. At $t = 14$s, an incremental fault in $P_h$ pressure sensor was invoked. This fault could not affect the multi-step tracking performance (Figure 13a) but it was mandatory to detect, isolate and identify the fault information and continue tracking with a fault alarm. The fault estimation was performed accurately as seen in Figure 13b. Figure 13c shows that, until $t = 14$s, pressure residuals for the UIOEFIR_pos and the UIOEFIR_pr were within the defined threshold $\varepsilon_{pr}(3) = \pm 5bar$. When the fault appeared the pressure residual of the UIOEFIR_pr did not cross the pre-set threshold as observed for the UIOEFIR_pos. This suggested that the fault occurred in $P_h$ pressure sensor and the corresponding fault-flag was set as 1 by *Algorithm 2* (Figure 13d). The overall state estimation performances under this sensor fault condition of UIOEFIR_pr and UIOEKF_pr are depicted in Figure 13(e-h). Figure 13e shows that the UIOEFIR_pr struggled to reduce the noise level while estimating the EHA velocity state. On the contrary, the estimated velocity obtained from the properly designed UIOEKF_pr was relatively better in this scenario. This can happen if the horizon length $N$ of UIOEFIR is set significantly lower than its optimal value (see Figure. 4). However, almost identical position estimation performance (Figure 13f) was achieved for both of the estimators. The head pressure $P_h$ estimation performance is depicted in Figure 13g. As seen, the designed UIOEFIR_pr showed higher accuracy compare to the UIOEKF_pr. Furthermore, an acceptable performance was also obtained by the presented UIOEFIR while estimating the rod-side pressure state $P_r$ of the EHA. Overall, except for the velocity estimation case, the under-optimal UIOEFIR estimated the EHA states at an adequate level compared to the high-accurately designed UIOEKF.

## VII. Conclusion

In this paper, an unknown input observer-combined EFIR estimator (UIOEFIR) is developed for solving the stochastic sensor fault and state estimation problem of an EHA with minimal design-effort. This has been achieved by adopting and UIO observer into the EFIR dynamics and hence, requirements of noise statistics are not necessary. To this end, an effective sensor FDA which can perform with any controller is developed using the proposed estimator to tolerate position and head-side pressure sensor fault of the EHA. In operation, the designed method effectively performed trajectory tracking by the conventional control logic and improved the estimation accuracy under time-varying measurement-noise. As the designed estimator is $N_{opt}$ times slower than the EKF-based method, techniques for reducing the computational cost will be investigated. Furthermore, future research will be carried out with actuator fault diagnosis in the FTC framework.

## Acknowledgement

This research was supported by Basic Science Program through the National Research Foundation of Korea (NRF) funded by the Ministry of Science and ICT, South Korea (NRF-2020R1A2B5B03001480). Authors also thank Warwick Manufacturing Group (WMG) and and WMG HVM Catapult, University of Warwick, UK for academic support.

## References

[1] X. Yang, X. Zheng and Y. Chen, "Position Tracking Control Law for an Electro-Hydraulic Servo System Based on Backstepping and Extended Differentiator," in IEEE/ASME Trans. Mechatronics, vol. 23, no. 1, pp. 132-140, 2018.

[2] W. Deng and J. Yao, "Extended-State-Observer-Based Adaptive Control of Electro-Hydraulic Servomechanisms without Velocity Measurement", in IEEE/ASME Trans. Mechatronics, 2019. Available: 10.1109/tmech.2019.2959297.

[3] J. Yao, Z. Jiao and D. Ma, "Extended-State-Observer-Based Output Feedback Nonlinear Robust Control of Hydraulic Systems With Backstepping," in IEEE Transactions on Industrial Electronics, vol. 61, no. 11, pp. 6285-6293, Nov. 2014.

[4] Z. Wang, P. Shi, C. C. Lim, "$H-/H_\infty$ fault detection observer in finite frequency domain for linear parameter-varying descriptor systems", Automatica, vol. 86, pp. 38-45, 2017.

[5] K. Zhang, B. Jiang and F. Chen, "MIMO Evolution Model-Based Coupled Fault Estimation and Adaptive Control With High-Speed Train Applications," in IEEE T CONTR SYST T, vol. 26, no. 5, pp. 1552-1566, 2018.

[6] H. Jeong, B. Park, S. Park, H. Min, S. Lee, "Fault detection and identification method using observer-based residuals", Reliability Engineering & System Safety, vol. 184, pp. 27-40, 2019.

[7] A. Qin, Q. Hu and Q. Zhang, "Concurrent Fault Diagnosis Based on Bayesian Discriminating Analysis and Time Series Analysis With Dimensionless Parameters," IEEE Sens. J., vol. 19, no. 6, pp. 2254-2265.

[8] Z. Wang, L. Liu and H. Zhang, "Neural Network-Based Model-Free Adaptive Fault-Tolerant Control for Discrete-Time Nonlinear Systems With Sensor Fault,", IEEE Transactions on Systems, Man, and Cybernetics: Systems, vol. 47, no. 8, pp. 2351-2362, 2017.

[9] Y. Wu, B. Jiang and N. Lu, "A Descriptor System Approach for Estimation of Incipient Faults With Application to High-Speed Railway Traction Devices", IEEE Trans. Syst., Man, Cybern: Systems, vol. 49, no. 10, pp. 2108-2118, 2019.

[10] Y. Wu, B. Jiang, Y. Wang, "Incipient winding fault detection and diagnosis for squirrel-cage induction motors equipped on CRH trains", ISA Transactions, Article in press, 2019. doi.org/10.1016/j.isatra.2019.09.020.
[11] Y. Wu, Z. Wang, Z. Huang, "Distributed fault detection for nonlinear multi-agent systems under fixed-time observer", Journal of the Franklin Institute, vol. 356, no. 13, pp. 7515-7532, 2019.
[12] A. Alzghoul, B. Backe, M. Löfstrand, A. Byström, B. Liljedahl, "Comparing a knowledge-based and a data-driven method in querying data streams for system fault detection: A hydraulic drive system application", Computers in Industry, vol. 65, no. 8, pp. 1126-1135, 2014.
[13] S. Ding, L. Xu, C. Su, "An optimizing method of RBF neural network based on genetic algorithm". Neural Comput & Applic, vol. 21, pp. 333–336, 2012.
[14] W. Shih-Ho, E. Wang, and P. Dorato, "Observing the states of systems with unmeasurable disturbances", IEEE Trans. Autom. Control, vol. 20, no. 5, pp. 716-717, 1975.
[15] J. Zarei, J. Poshtan., "Sensor Fault Detection and Diagnosis of a Process Using Unknown Input Observer", vol. 16, no. 1, pp. 31-42, 2011.
[16] M. Liu, L. Zhang, P. Shi and Y. Zhao, "Fault Estimation Sliding-Mode Observer with Digital Communication Constraints", IEEE Trans. Autom. Control, vol. 63, no. 10, pp. 3434-3441, 2018.
[17] S. K. Kommuri, S. B. Lee and K. C. Veluvolu, "Robust Sensors-Fault-Tolerance with Sliding Mode Estimation and Control for PMSM Drives," in IEEE/ASME Trans. Mechatronics, vol. 23, no. 1, pp. 17-28.
[18] L. Liu, Y. Liu, D. Li, S. Tong and Z. Wang, "Barrier Lyapunov Function-Based Adaptive Fuzzy FTC for Switched Systems and Its Applications to Resistance-Inductance-Capacitance Circuit System", IEEE Trans. Cybern., pp. 1-12, 2019.
[19] L. Liu, Y. Liu and S. Tong, "Neural Networks-Based Adaptive Finite-Time Fault-Tolerant Control for a Class of Strict-Feedback Switched Nonlinear Systems", IEEE Trans. Cybern., vol. 49, no. 7, pp. 2536-2545.
[20] Z. Wang, Y. Wu, L. Liu and H. Zhang, "Adaptive Fault-Tolerant Consensus Protocols for Multiagent Systems With Directed Graphs", IEEE Transactions on Cybernetics, vol. 50, no. 1, pp. 25-35, 2020.
[21] Fu, X.B., "Fault diagnosis of hydraulic system in large forging hydraulic press". Measurement, vol. 49, pp. 390-396, 2014.
[22] A. Schwung, M. Beck, and J. Adamy, Fault diagnosis of dynamical systems using recurrent fuzzy systems with application to an electrohydraulic servo axis. Fuzzy Sets and Systems, 2015. vol. 277, pp. 138-153.
[23] R. M. Asl, Y. S. Hagh, S. Simani, H. Handroos, "Adaptive square-root unscented Kalman filter: An experimental study of hydraulic actuator state estimation", Mech Syst Signal Process., vol. 132, pp. 670-691, 2019.
[24] K. Salahshoor and M. Mosallaei, "Centralized and decentralized process and sensor fault monitoring using data fusion based on adaptive extended kalman filter algorithm, Measurement", 2008. 41 (10): p. 1059–1076.
[25] S. Gautam, P. K. Tamboli, K. Roy, V. H. Patankar, S. P. Duttagupta, "Sensors incipient fault detection and isolation of nuclear power plant using extended Kalman filter and Kullback–Leibler divergence", ISA Transactions, vol. 92, pp. 180-190, 2019.
[26] P. Halder, "A Novel Approach for Detection and Diagnosis of Process and Sensor Faults in Electro-Hydraulic Actuator," Int. J. Engineering Research and Development, Vol. 6, No. 7, p. 15-22, 2013.
[27] S. A. Nahian, D. Q. Truong, P. Chowdhury, "Modeling and fault-tolerant control of an electro-hydraulic actuator". Int. J. Precis. Eng. Manuf, 2016. 17(10): p. 1285–1297.
[28] Y. Li, M. Zhong, "Fault estimation for discrete-time singular systems with random sensor failures.", IFAC-PapersOnLine, vol. 48, no. 21, pp. 701-706, 2015.
[29] Y. S. Shmaliy, "An iterative Kalman-like algorithm ignoring noise and initial conditions", IEEE Trans. Signal Process, vol. 59, pp. 2465–2473.
[30] Y. S. Shmaliy, "Suboptimal FIR Filtering of Nonlinear Models in Additive White Gaussian Noise", IEEE Transactions on Signal Processing, vol. 60, no. 10, pp. 5519-5527, 2012.
[31] S. Zhao, Y. S. Shmaliy and F. Liu, "Fast Kalman-Like Optimal Unbiased FIR Filtering With Applications", IEEE Transactions on Signal Processing, vol. 64, no. 9, pp. 2284-2297, 2016.
[32] J. P Franquiz, S. H. Khan, and Y.S. Shmaliy, "Combined extended FIR/Kalman filtering for indoor robot localization via triangulation", Measurement, vol. 50, pp. 236-243, 2014.
[33] Y. Xu; Y. S. Shmaliy; C. K. Ahn; G. Tian; X. Chen, "Robust and accurate UWB-based indoor robot localisation using integrated EKF/EFIR filtering". IET RADAR SONAR NAV, vol. 12, no. 7, pp. 750 – 756, 2014.
[34] M. H. Sobhani, J.P., "Fault detection and isolation using unknown input observers with structured residual generation. International Journal of Instrumentation and Control Systems vol. 2, no. 2, pp.1-12, 2012.
[35] J. Chen, R. J. Patton, and H. Y. Zhang, "Design of unknown input observers and robust fault detection filters", International Journal of Control, vol. 63, no. 1, pp. 85-105, 1996.
[36] R. M. Murray, Z. Li, S. S. Sastry, S. S. Shankara, "Lyapunov Stability Theory" in A Mathematical Introduction to Robotic Manipulation, CRC press, 1994, ch. 4, pp. 179–187.
[37] J. P. Hespanha, A. S. Morse, "Switching between stabilizing controllers", Automatica, vol. 38, no. 11, pp. 1905-1917, 2002.
[38] X. Meng, L. Xie, Y. C. Soh, "Reset control for synchronization of multi-agent systems", Automatica, vol. 104, pp 189-195, 2019.
[39] M. R. Homaeinezhad, S. Yaqubi, "Adaptive Fuzzy-Wavelet Neural Network identification core for reinforced control of general arbitrarily switched nonlinear Multi Input-Multi Output Dynamic Systems", Applied Soft Computing, vol. 91, pp. 1-26, 2020.

**Syed Abu Nahian** received his B.Sc in Mechanical Engineering from Chittagong University of Engineering and Technology (CUET), Bangladesh and Ph.D. degree in Mechanical and Automotive Engineering from University of Ulsan, S. Korea in 2010 and 2017 respectively. In 2018, He joined as an Assistant Professor (Research) in the Institute of Energy Technology, CUET. In Oct. 2019, He joined in WMG, Univ. of Warwick, UK as a Project Engineer. His current research interests are Electric/Hybrid propulsion, Fault diagnosis, Energy-Mechatronics & Control-Applications.

**Dinh Quang Truong** got the first-class B.E. mechatronics degree in the Mechanical Engineering Department at Hochiminh City University of Technology, Vietnam in March 2006. In 2010, he obtained Ph.D. degree from the School of Mechanical Engineering at University of Ulsan, South Korea. He worked as a postdoctoral researcher and as a research professor at the same university for several years. Currently he is an Assistant Professor of WMG, University of Warwick, UK. His current research interests include Energy-systems and control.

**Hoang Vu Dao** received the B.E. mechatronics degree in School of Mechanical Engineering at Hanoi University of Science and Technology, Vietnam in July 2018. He is currently working toward the Ph.D. degree in mechanical engineering with the School of Mechanical Engineering, University of Ulsan, Ulsan, South Korea. His current research interests include hydraulic robot, nonlinear control and fault-tolerant control.

**Kyoung Kwan Ahn** received the B.S. and M.Sc degree in Mechanical Engineering from Seoul National University, Seoul, Korea (1990) and Korea Advanced Institute of Science and Technology (KAIST), Daejeon, Korea (1992) respectively. In 1999, He obtained Ph.D. degree from the Tokyo Institute of Technology, Tokyo, Japan. He is currently a Professor in the School of Mechanical Engineering, University of Ulsan, Korea. His research interests include design and control of smart actuators, fluid power control, and active damping control.